Chapter 6
Pressure Probes

Michael Nicklas

Abstract The physical properties of correlated materials, like low-dimensional organic conductors, cuprate superconductors, heavy-fermion metals, or the recently discovered iron-based superconductors, depend on a delicate interplay of different physical effects. External pressure is an ideal tool to tune this interplay. The resulting phase diagrams and their study is essential for the understanding of the underlying physical principles. This chapter is intended to give an introduction to modern pressure techniques which are used for investigations of strongly correlated materials. We provide a short overview of the different types of pressure cells. Thereby, we focus on the experimental capabilities and point at limits and problems which might occur in a pressure experiment. In a survey of experimental probes we outline the specifics of the experimental setup for pressure studies in comparison with the setup used at ambient pressure. We further address the particular restrictions on the experimental resolution in the pressure study and discuss the accessible parameter range in pressure, temperature and magnetic field. The covered physical probes include, electrical- and thermal-transport measurements, thermodynamic and magnetic studies, magnetic-resonance experiments, and structural and spectroscopic investigations. On the example of heavy-fermion superconductors we elucidate the contributions of pressure experiments on the discovery and understanding of new emerging physical phenomena in correlated electron materials.

6.1 Introduction

External pressure is an excellent tool to tune the interplay of different energy scales in strongly correlated materials in a clean and controlled way. One notable example for competing interactions is the magnetic Ruderman-Kittel-Kasuya-Yoshida (RKKY) exchange interaction and the Kondo effect in heavy-fermion metals. The major drawback of *pressure probes* is the additional complexity of the experiments due to the

M. Nicklas (✉)
Max Planck Institute for Chemical Physics of Solids,
Nöthnitzer Str. 40, 01187, Dresden, Germany
e-mail: nicklas@cpfs.mpg.de

A. Avella and F. Mancini (eds.), *Strongly Correlated Systems*,
Springer Series in Solid-State Sciences 180, DOI 10.1007/978-3-662-44133-6_6

pressure cells needed to generate the high pressure. Today, many physical quantities are accessible at high pressures. Available probes comprise, for example, electrical transport, thermodynamic and magnetic properties, but also magnetic resonance and scattering techniques. Compared to ambient-pressure measurements, the accessible temperature range might be limited and the sensitivity of the experiment reduced.

In this chapter we will concentrate on the experimental techniques adapted to high-pressure environments. In Sect. 6.2 we give an overview on different types of pressure cells with a focus on pressure cells which are currently used in the laboratories. In the following section (Sect. 6.3) we describe the different ways to determine the actual pressure inside the pressure cell and discuss the importance of the pressure transmitting medium in carrying out a successful experiment. In Sect. 6.4 we provide a survey of the implementation of the measurement of different physical quantities in pressure cells. We put our special attention on the particular requirements in the study of correlated electron materials. Our aim is to point out the modifications of experimental setups and the limitations and problems which can occur while performing pressure experiments. A discussion of technical details is beyond this introductory text, therefore, we refer to the literature at the appropriate places. In the final section (Sect. 6.5) we highlight the importance of pressure studies on the example of heavy-fermion materials.

6.2 Pressure Generation

The target of a pressure study is to measure a physical quantity at high pressures with the same sensitivity as at ambient pressure. This is usually difficult due to the fact that the sample and eventually the experimental setup have to be placed inside the pressure cell, which provides only a limited space. The size of the pressure chamber can be of the order of a few hundred micrometers up to several millimeters in diameter depending on the type of pressure cell. There are additional restrictions connected to the specific type of a physical investigation, for example, it might be difficult to reach low temperatures ($T \ll 1\,\mathrm{K}$) and high magnetic fields with a pressure setup.

6.2.1 Pressure Cells

In the following, we give an introduction to high-pressure techniques and present the different types of pressure cells which are used to investigate strongly correlated materials. The main challenge of pressure experiments becomes evident when we write pressure (p) as:

$$p = \frac{F}{A}, \tag{6.1}$$

where F is the force acting on the area A. To increase the maximum achievable pressure of a pressure setup, we can follow two routes: (i) generate larger and larger forces or (ii) reduce the size of the sample chamber further and further. The first route, which is, for example, followed in the field of earth sciences or high-pressure materials synthesis, requires the use of a large hydraulic press and corresponding pressure apparatus. Due to the size of the whole setup this route is not appropriate for low-temperature experiments, which require small pressure cells fitting in a cryostat. On the other hand, going to smaller and smaller dimensions is also no ideal solution, since it becomes more and more challenging to set up an experiment due to the reduced size of the sample chamber. Despite of these challenges, usually the second route is followed to study the physical properties of materials at high pressures.

In general, pressure cells can be divided into different groups depending on their mechanism adapted to generate the pressure [1]. Most commonly used in laboratories are the piston-cylinder type and opposed-anvil type pressure cells. While the maximum pressure in piston-cylinder type cells is limited to about 4 GPa, in diamond-anvil cells (DAC's) pressures well above 100 GPa can be reached. The interesting physics in strongly correlated materials, like pressure-induced superconductivity or quantum critical phenomena, is in most cases observed in the pressure range below 10 GPa.

6.2.2 Piston-Cylinder Type Pressure Cells

Piston-cylinder type pressure cells have the advantage of a reasonably large volume sample chamber and a relatively small size. This enables pressure studies of a large number of physical properties, like electrical transport, heat capacity, magnetic probes, neutron scattering, etc., down to very low temperatures and in high magnetic fields. This type of cell is easy to handle and, therefore, in use in many laboratories. The name *piston-cylinder* type pressure cell comes from the moving piston inside the pressure cylinder, on which the force is applied to compress the sample chamber. To apply the force a hydraulic press is used. After application of the desired force, the pressure inside the cell is clamped with a locking nut. For this reason, also the term *clamp-type* pressure cell is used. Afterwards, the cell can be placed inside the cryostat. For measurements in magnetic fields pressure cells machined from magnetic materials are not suitable. Therefore, a nonmagnetic Cu:Be alloy with about 2.5 % Be is used as material for the cell body. Compared with maraging steel, also used as a material for constructing pressure cells, Cu:Be has the advantage that it is nonmagnetic and still has a reasonably high tensile strength ($\sim$1.3 GPa). Considering the hassles accompanying the usage and machining of alloys containing beryllium, Cu:Ti may become an alternative material for pressure cells [2].

The maximum pressure generated using a Cu:Be piston-cylinder type pressure cell is limited to about 1.5 GPa. Above this pressure plastic deformations take place. In Cu:Be cells with a particular small volume sample chamber higher pressures can be achieved on the expense of a plastic deformation of the pressure chamber. Double-layer piston-cylinder type cells have been invented to reach higher pressures and to

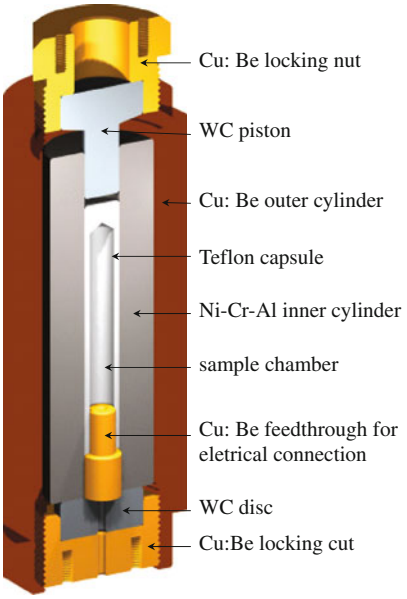

Fig. 6.1 Schematic drawing of a double-layer piston-cylinder type pressure cell. The outer diameter of this cell is about 25 mm. Using this or similar designs pressures between 3 and 4 GPa can be reached

maintain a large volume sample chamber [3]. In a double-layer piston-cylinder type cell pressures between 3 and 4 GPa can be reached [3–6]. Furthermore, this type of cell is extremely versatile and can be used for different kinds of experiments. A schematic drawing of a typical design is displayed in Fig. 6.1. The cell consists of an outer cylinder machined of Cu:Be and an inner cylinder of Ni-Cr-Al, which has a higher tensile strength than Cu:Be [2]. Instead of Ni-Cr-Al also MP35N, a Co-Ni-Cr-Mo alloy, is often used as material for the inner cylinder [2]. Its magnetic properties due to the Co content make its use less favorable.

6.2.3 Opposed-Anvil Type Pressure Cells

The class of opposed-anvil pressure cells comprises many different types of cells. The highest pressures can be reached with the diamond-anvil cell (DAC), but this offers the smallest available sample space. Other types of opposed-anvil cells, like the Bridgman-type cell or the toroidal-anvil cell, have a larger available space for the sample, but do by far not reach the maximum pressures of DAC's.

The general principle of an opposed-anvil type pressure cell is illustrated in Fig. 6.2. One of the anvils is usually fixed in place and the force is applied to the movable anvil. The gasket sits in between the anvils and seals the pressure inside the

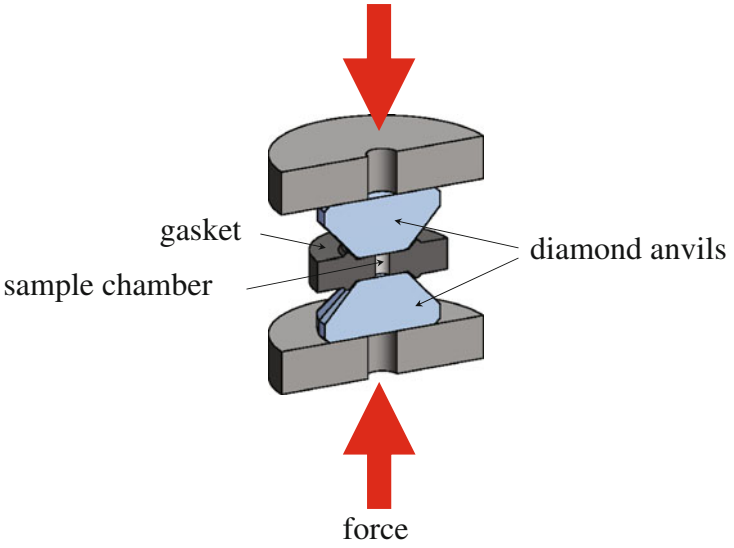

Fig. 6.2 Schematic representation of the principle of an opposed-anvil cell illustrated on the example of a diamond-anvil pressure cell (DAC)

sample chamber filled with the pressure transmitting medium and the sample(s). Next to the sample(s) a pressure gauge is placed in order to determine the pressure inside the sample chamber (see Sect. 6.3). In most setups, the pressure is changed at room temperature using a hydraulic press and then clamped by one or more screws (nuts). In addition to the application of pressure at room temperature, in some experimental setups the pressure can be changed at low temperatures using a bellow system [7, 8].

The clamped Bridgman-type anvil technique has the most simple setup. Usually tungsten carbide (WC) serves as material for the anvils, but sometimes sintered synthetic diamond is used to reach higher pressures. While WC starts to deform above 11 GPa, limiting the maximum pressure which can be obtained with these anvils, sintered synthetic diamond allows to reach pressures up to 30 GPa. The sintered synthetic diamond anvils are magnetic which limits their usability in some experiments. In contrast to sintered synthetic diamond, non-magnetic WC is available. The remnant field of a magnetic anvil after an experiment in magnetic fields can, for example, shift the superconducting transition of lead used as manometer to lower temperatures leading to an overestimation of the pressure inside the cell (see Sect. 6.3.1). Figure 6.3 shows an electrical-resistivity setup in a Bridgman-type pressure cell. The gasket consists of pyrophyllite (a sheet silicate) and the samples sit in between two sheets of the soft mineral steatite, which is in this case the pressure transmitting medium (see Sect. 6.3.2). With this experimental setup the resistivity of two samples and lead, which serves as pressure gauge, can be measured at the same time (see also Sects. 6.3.1 and 6.4.1).

The solid pressure transmitting medium causes non-isotropic pressure distributions in the sample chamber. To obtain more isotropic pressure conditions in

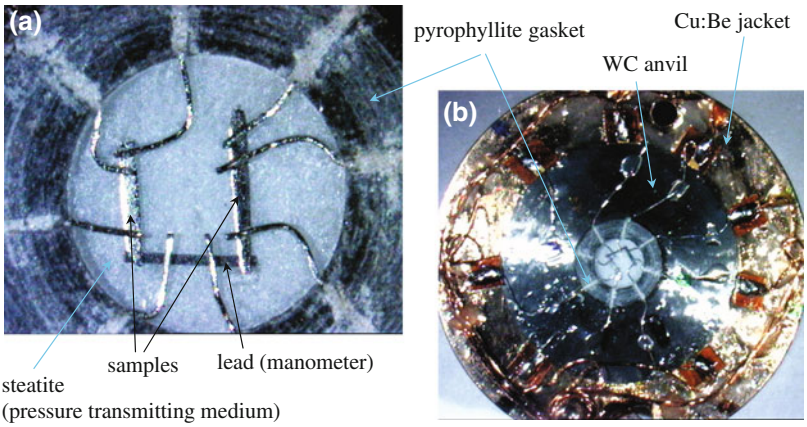

Fig. 6.3 **a** Setup for electrical-resistivity measurements in a Bridgman-type pressure cell. The sample chamber has a diameter of 2 mm. Before closing the cell a second steatite disc will be placed on top of the samples. **b** WC anvil enclosed in a Cu:Be jacket. Pyrophyllite serves as material for the gasket [9]

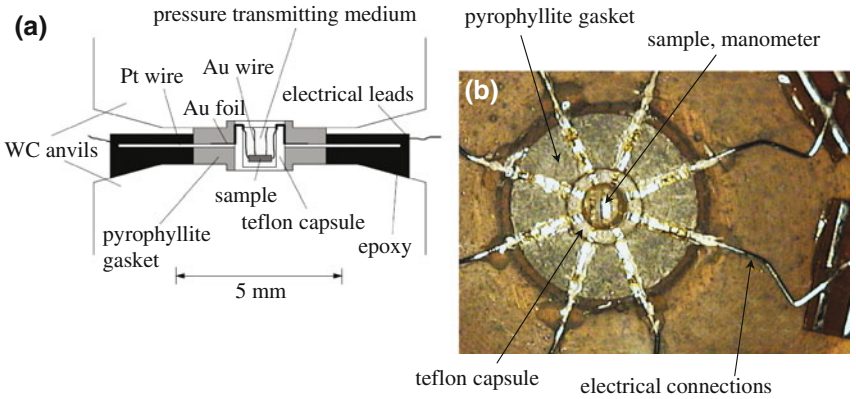

Fig. 6.4 Schematic drawing (**a**) and photograph (**b**) of modified Bridgman anvils with an experimental setup for electrical-resistivity studies. A liquid is used as pressure transmitting medium (see also [10–12])

Bridgman-type pressure cells different attempts have been made to replace steatite by a liquid pressure transmitting medium. One procedure is to impregnate the inner wall of the gasket with epoxy [13]. Another one uses teflon rings as sealing in a classical Bridgman setup [14]. A completely different approach uses modified anvils and a teflon capsule as pressure chamber [10–12]. An example for such a setup is shown in Fig. 6.4. In this cell pressures of about 8 GPa can be reached using a liquid pressure transmitting medium. A similar design has been realized in toroidal-anvil cells [15–17]. The maximum achievable pressure and the available sample space are comparable in both types of pressure cells.

In a diamond-anvil cell the highest possible static pressure can be achieved. This requires a very high precision of the alignment of the opposed diamond anvils. The major drawback of the DAC technique is the limited experimental space of the order of only a few 100 μm in diameter and several 10 μm in height, depending on the size of the diamonds used. A brief history of the DAC, which was invented more than 50 years ago, is given in an article by Basset [18]. Further useful information on technical aspects can be found in [19–21].

Even though, pressures far beyond 100 GPa can be obtained in DAC's, the experimental methods for pressures larger than 50 GPa are typically limited to physical probes which do not need electrical connections inside the pressure chamber, but take advantage of the transparency of diamonds in a large frequency range. These methods include optical spectroscopy, X-ray scattering/spectroscopy, or Mössbauer spectroscopy. For other probes, like electrical transport or specific heat, the main challenge is to bring electrical connections into the high-pressure region. Today, DAC's have been miniaturized so far that they can be used in most standard laboratory cryogenic systems. Examples for different DAC designs can be found in [22–25].

6.2.4 *Indenter-type Pressure Cells*

With indenter-type pressure cells pressures up to 4.5 GPa at low temperatures have been reached using a liquid pressure transmitting medium [26]. This pressure is above the limit of piston-cylinder type cells. Furthermore, the indenter type cell still provides a reasonably sized sample space of about 1.6 mm in diameter and 1.4 mm in depth, which is reduced to 0.7 mm at the maximum pressure. A schematic drawing is shown in Fig. 6.5. In some respects, this pressure cell can be considered

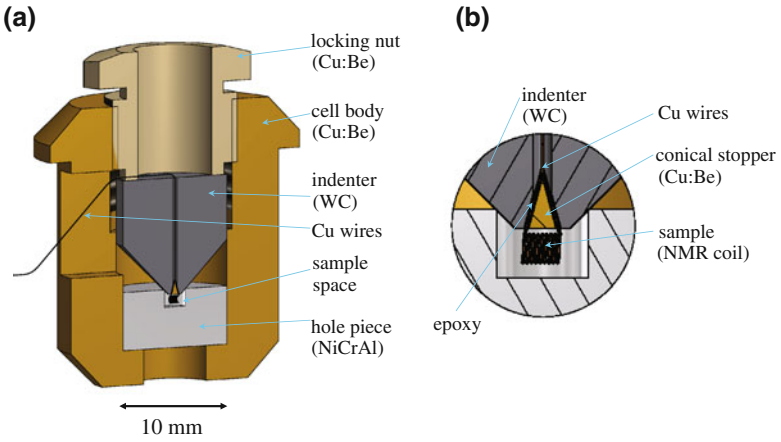

Fig. 6.5 *left* Cross-sectional view of the indenter pressure cell. *right* Arrangement for nuclear magnetic resonance (NMR) measurements in the indenter cell (after [26])

as the upper part of an opposed-anvil cell, just the lower anvil and the gasket are missing and replaced by a piece of Ni-Cr-Al with a hole serving as sample chamber. A main advantage compared to modified Bridgman or toroidal-anvil cells is that the feedthrough for the electrical wires can be reused. However, the piece with the hole is deformed in the experiment and has to be replaced each time.

6.2.5 Other Types of Pressure Cells

We briefly want to mention two further types of pressure cells. The multi-anvil pressure cells are fairly complicated to operate, since the whole setup, including a custom-made cryostat, is placed inside a large hydraulic press [27, 28]. Due to the construction the temperature is limited to the range of a ^{4}He cryostat. The helium gas pressure cells are the second type of pressure cells we want to refer to. In them pressures up to about 1.7 GPa can be reached. However, practically the pressure is limited to 1 GPa because of the safety limits of the available pressure fittings. Due to the usage of helium gas as pressure transmitting medium the helium gas pressure cells offer excellent hydrostatic pressure conditions and a very good pressure control especially at small pressures [29, 30].

6.2.6 Electrical Connections

Several experimental probes require electrical connections inside the pressure chamber. This provides an additional challenge for the experimentalists. The electrical connections are usually the first place where a pressure experiment fails, e.g. due to a short circuit to the ground. For piston-cylinder type pressure cells quite reliable electrical feedthroughs can be prepared using glass or sapphire filled epoxies [3]. To prepare reliable electrical connections for anvil cells using metallic gaskets is more difficult. The wires have to be electrically insulated from the gasket. This can be done by covering the gasket by sapphire (Al_2O_3) or cubic boron nitride (CBN) powder mixed with epoxy. However, there is a high risk of an electrical short circuit while closing the cell and applying pressure, e.g. at the edges of the gasket. A promising way to overcome this obstacle of the anvil cells, are patterned anvils [31–33]. Here, electrical leads or even more complicated structures like multilayered coils for magnetic measurements are deposited on the anvil and consecutively covered by an additional layer of the anvil material. One problem in experiments can arise from the poor electrical properties of the materials which can be used for depositing the structures. Figure 6.6 shows examples of electrical contact leads and a multilayered coil evaporated on sapphire (Al_2O_3) and moissanite (single-crystalline SiC) anvils [34].

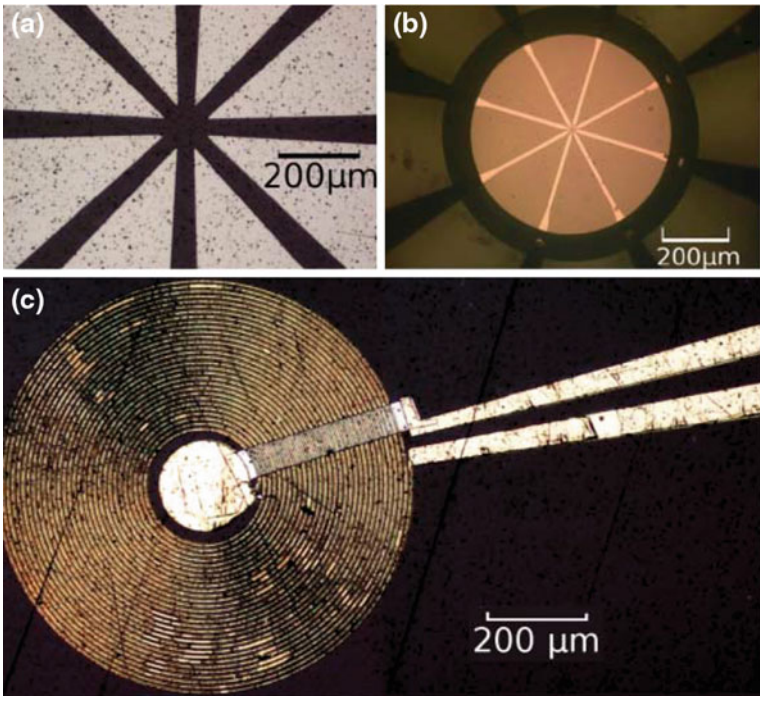

Fig. 6.6 Patterned anvil designs. **a** Al_2O_3 anvil with eight lead probe pattern **b** moissanite (single-crystalline SiC) anvil with eight-lead probe NiCr pattern, and **c** Au on NiCr multilayered coil pattern on an Al_2O_3 anvil [31]. *Reproduced with permission from Review of Scientific Instruments 82, 033901 (2011). Copyright 2011 American Institute of Physics*

6.3 Pressure Determination and Transmitting Media

The exact determination of the pressure and the quality of the pressure conditions inside a pressure cell are very important for any high-pressure experiment.

6.3.1 Pressure Determination

A simple estimation of the pressure inside the pressure cell as applied force per surface area (6.1) is not reliable. Due to friction effects the actual force transmitted to the sample space is not known exactly. Furthermore, the surface area of the pressure chamber can change with pressure, especially, in opposed anvil cells. Therefore, more precise pressure gauges placed next to the sample inside the pressure chamber are needed.

An other important point to consider in a pressure experiment is that due to the different thermal expansions of the materials used in the pressure cell setup, i.e. for the pressure cell body, pistons or anvils, pressure transmitting medium etc., the

pressure inside the pressure cell increases or decreases on cooling. Even though, the design of a pressure cell can compensate this effect partly, it is important to be aware that the pressure inside a pressure cell is never constant on changing temperature. Therefore, it is important at which temperature the pressure inside the pressure cell is determined.

Depending on the type of pressure cell different manometers are available. The pressure dependence of the electrical resistance of Manganin wire can be utilized as pressure gauge [35–38]. Due to the mainly temperature independent resistance, Manganin can be used in a large temperature range. The linear pressure dependence of the electrical resistivity of manganin is very reproducible and can be calibrated using the structural transitions of bismuth under pressure. These are easily detectable in the electrical resistance and serve as reliable fix points for a calibration [39, 40].

Another widely deployed method to determine the pressure at low temperatures uses the strong pressure dependencies of the superconducting transition temperatures (T_c) of lead, tin, or indium [41, 42]. For pressures up to 5 GPa the following relations hold (p in GPa) [41]:

$$\begin{aligned} \text{Pb}: \quad & T_c(p) = T_c(0) - (0.365 \pm 0.003)\,p, \\ \text{Sn}: \quad & T_c(p) = T_c(0) - (0.4823 \pm 0.002)\,p + (0.0207 \pm 0.0005)\,p^2, \\ \text{In}: \quad & T_c(p) = T_c(0) - (0.3812 \pm 0.002)\,p + (0.0122 \pm 0.0004)\,p^2. \end{aligned} \tag{6.2}$$

Here, no additional calibrations are needed and T_c can be determined by electrical resistance or magnetic susceptibility (magnetization). The latter has the advantage that no electrical connections inside the pressure chamber are required. We note, one important drawback of this method is that the T_c of lead, tin, or indium is highly sensitive to a magnetic field. Thus, the remnant field of a superconducting magnet in a typical experimental setup can already lead to a strong shift of T_c to lower temperatures, pretending a much higher pressure inside the cell. Therefore, it is important to remove any remnant field carefully (to less than 0.1 mT) before using this method as pressure gauge. The width of the superconducting transition can also serve as a measure of the pressure gradient inside the pressure chamber by taking the size of the manometer into account.

In diamond-anvil cells, or more generally, in pressure cells with optical access, the pressure shift of the ruby fluoresce line R_1 is used as pressure gauge [43, 44]. This method is not limited to a certain temperature range. Furthermore, the placement of several ruby grains inside the pressure chamber, which can be individually focused by an optics, allows for a detailed study of the pressure gradient. The pressure (p in GPa) can be obtained from the R_1 line-shift [45–47]:

$$p = \frac{1904}{B}\left[\left(1 + \frac{\delta\lambda}{6.9424}\right)^B - 1\right], \tag{6.3}$$

with $\delta\lambda$ the line-shift of the ruby R_1 line in nm and the parameter B as a measure of the hydrostaticity ($B = 7.665$ for hydrostatic conditions).

In addition to the previously described methods, there are further ways to determine the pressure, which are directly related to a particular physical probe. In the case of nuclear quadrupol resonance (NQR) or nuclear magnetic resonance (NMR) experiments the pressure shift of the ^{63}Cu NQR spectrum of Cu_2O is established as pressure gauge [48, 49]. Here, a Cu_2O piece is placed inside the detection coil, next to the sample under investigation (see also 6.4.7.1). Furthermore, X-ray and neutron diffraction experiments allow to utilize the equation of state (EOS), e.g. of NaCl, to determine the pressure [50].

6.3.2 Pressure Transmitting Media

Ideal isotropic pressure conditions cannot be achieved in real pressure experiments. Nevertheless, the quality of the pressure conditions inside the pressure cell can be crucial for the success of an experiment. Non-hydrostatic effects, e.g. uniaxial strain, can strongly influence the physical properties of a sample. Therefore, it is important to carefully choose an appropriate pressure transmitting medium. A gas, like Ar or He, offer the best isotropic pressure conditions. However, we want to point out that even a solid pressure transmitting medium like steatite, AgCl, or NaCl can provide satisfactory pressure conditions depending on the samples and physics investigated. On the other hand, even the solidification of helium can cause anomalies in the data of very strain sensitive materials [51]. Therefore, in case unexpected anomalies appear in the data, it is important to look at the properties of the pressure transmitting medium, e.g. solidification pressure or temperature. A recent study reports on the properties of many commonly used pressure transmitting media [52]. This study covers the pressure range up to 10 GPa in different temperature regions. Further information can be also found in [53–62].

6.4 Physical Probes

6.4.1 Electrical Transport

The electrical resistance is probably the most used probe to investigate the physics of strongly correlated materials under pressure. This is because the electrical resistance, including magnetoresistance and Hall-effect, is the only physical property which can be measured with the same precision, in almost the same temperature and magnetic field range, under pressure like at ambient conditions. All other probes suffer from higher background contributions, reduced sensitivities, or other limiting factors.

In a piston-cylinder type pressure cell several samples can be measured in one experiment. A typical setup for three samples and the pressure gauge is shown in Fig. 6.7. In opposed-anvil cells only one or two samples can be investigated simulta-

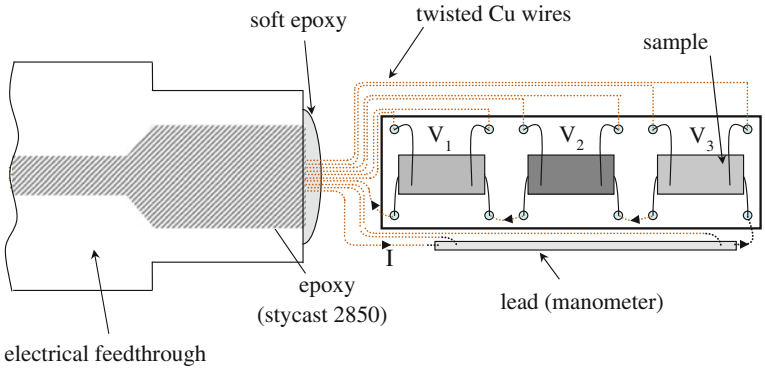

Fig. 6.7 Electrical feedthrough for a piston-cylinder type pressure cell with sample board. The electrical wiring is shown schematically for 3 samples and the pressure gauge (strip of lead). A serial electrical current is used for all samples

neously (see also Fig. 6.3). In electrical-resistance experiments maximum pressures of above 50 GPa can be achieved in DAC's.

6.4.2 Thermal Transport and Thermoelectric Power

6.4.2.1 Thermal Transport

Thermal transport is difficult to measure inside a pressure cell. In contrast to ambient pressure experiments, where the sample sits in vacuum, the heat loss from the sample to the pressure medium is generally significant and makes any measurement of the thermal conductivity using the steady-state method under pressure nearly impossible [63]. To overcome this problem two different methods have been proposed, the transient method [64, 65] and the 3ω method [66]. The latter has the advantage that very small samples can be measured. The small sample size and the high measurement frequencies help to reduce the heat loss from the sample to the pressure medium. However, the losses cannot be neglected. This method is limited to intermediate temperatures ($T \gtrsim 10\,\mathrm{K}$).

6.4.2.2 Thermoelectric Power

In contrast to thermal transport, the measurement of the thermoelectric power (TEP), S, is well established under pressure [67–69]. To measure $S(T)$ a temperature gradient is induced across the sample. S is defined as:

$$S(T, p) = \frac{\Delta T(T, p)}{\Delta V(T, p)}, \tag{6.4}$$

where ΔT is the thermal gradient and ΔV the thermoelectric voltage across the sample. The temperature gradient is usually measured using thermocouples as thermometers. For the determination of S from the experimental data the knowledge of the absolute values of the TEP of the material used for the voltage leads and its pressure dependence is essential [70]. In pressure experiments different setups with one or two thermocouples are used. In the former case it is assumed that the cold end of the sample is at the temperature of the bath [69]. The sensitivity of the available thermocouples limits the experiments to the temperature range above 1 K. TEP experiments have been carried out up to 30 GPa in Bridgman-type pressure cells using steatite as pressure transmitting medium [69, 71]. In DAC's a combination of ZrO_2 and CsI is used as pressure transmitting medium which also serves as a thermal insulation of the sample from the diamond anvils [72]. Piston-cylinder type pressure cells have been also successfully deployed for TEP experiments [68, 73].

6.4.3 Heat Capacity

For studies of the heat capacity under pressure two approaches are followed. The first method provides absolute values of the heat capacity by measuring the heat capacity of the whole pressure cell with the sample inside. A subtraction of the addenda finally yields the heat capacity of the sample. Following the second procedure semi-quantitative data is obtained by using an ac-technique to directly measure the heat capacity of the sample inside the pressure cell.

Using the first technique, the heat capacity of the whole pressure cell with the sample inside is measured [77–79]. To obtain the specific heat of the sample, the addenda, including the contributions of the pressure cell and the pressure trans-

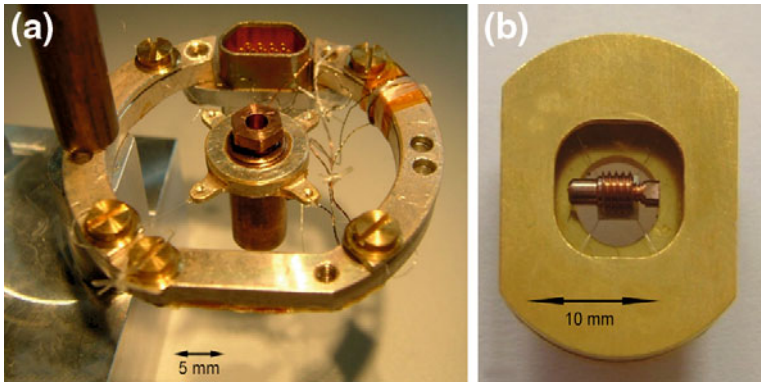

Fig. 6.8 Two different pressure cells for heat-capacity measurements. **a** Setup for a dilution refrigerator, **b** miniature cell on a commercial heat-capacity platform [74–76]

mitting medium, has to be carefully determined and subtracted from the raw data [77–79]. Depending on the size of the pressure cell a customized measurement rig or a standard heat-capacity platform is employed (see Fig. 6.8). The heat capacity is then determined by a quasi-adiabatic heat-pulse technique [80] or a relaxation technique [81, 82]. The main limitation of this method is that only samples with a large heat capacity compared with the heat capacity of the pressure cell can be investigated. Furthermore, only piston-cylinder type pressure cells provide a large enough volume for the sample, but limit the maximum achievable pressures to the 3 GPa range. One class of materials suited for this method are the heavy-fermion materials. In a pressure experiment the heat capacity of a heavy-fermion sample typically reaches between 10 and 120 % of the heat capacity of the pressure cell. At higher temperatures the contribution of the pressure cell to the total heat capacity increases stronger than that of the sample, making measurements above ∼10 K basically impossible. Experiments starting from temperatures below 50 mK can be carried out. However, in the low-temperature range ($T \lesssim 0.5$ K) nuclear Schottky contributions to the heat capacity, e.g. from the Cu in the pressure cell, become substantial in magnetic fields. Since these contribute significantly to the addenda, precise measurement in high magnetic fields and at low temperatures are very challenging.

The second available method, the ac-technique directly measures the heat capacity of the sample and can, therefore, be adapted to different types of pressure cells. It allows to study small crystals since thermometer and resistive heater are usually directly glued to the sample [83, 84]. For diamond-anvil cells also a laser heating method has been developed [85]. For the ac-technique the thermal conduction inside the sample has to be much larger than that from the sample to the surrounding pressure medium. In practice this can be achieved by choosing an appropriate sample geometry and measurement frequency. As thermometer a thermocouple is usually the best choice. Due to its small thermal mass it follows the temperature of the sample immediately. The sensitivity of thermocouples strongly decreases with decreasing temperature. In the low-temperature region (<1 K) AuFe/Au thermocouples give the best sensitivity [70]; at temperatures above 2 K Au/Chromel thermocouples provide a good resolution [70, 85]. Below 300 mK the resolution of the thermocouples decreases rapidly making ac-heat-capacity experiments more and more difficult. The ac-technique has been adapted for different types of pressure cells, e.g. piston-cylinder type pressure cells [86, 87], Bridgman-type cells with solid [70, 88, 89] and liquid pressure medium [71], cubic-anvil setups [90], and diamond-anvil cells [85].

6.4.4 Thermal Expansion and Magnetostriction

The linear thermal expansion, respectively, the volume thermal expansion coefficient,

$$\alpha = \frac{1}{\ell(T)} \cdot \frac{\partial \ell(T)}{\partial T} \text{ and } \beta = \frac{1}{V_s(T)} \cdot \frac{\partial V_s(T)}{\partial T}, \tag{6.5}$$

and the magnetostriction coefficient,

$$\lambda = \frac{1}{\ell(B)} \cdot \frac{\partial \ell(B)}{\partial B}, \tag{6.6}$$

are important thermodynamic properties suitable for studying different types of phase transitions. Here, ℓ is the length and V_s the volume of the sample.

Under pressure there are only two ways to determine the thermal expansion/magnetostriction coefficient: (i) a study of the lattice parameters by X-ray or neutron diffraction (see also Sect. 6.4.8) or (ii) the strain-gauge technique [15, 91, 92]. The first method does not only provide α and β, but also gives structural information, e.g. the pressure dependence of the lattice parameters (see for example [93]). Furthermore, fitting the unit-cell volume, $V(p)$, using the second order Murnaghan's equation of state (EOS),

$$p = \frac{B_0}{B_0'} \left[\left(\frac{V_0}{V(p)} \right)^{B_0'} - 1 \right], \tag{6.7}$$

gives the bulk modulus, B_0, of the material. B_0' is a parameter, which is typically between 3 and 6 in intermetallic compounds, and V_0 is the unit-cell volume at ambient pressure. The second way to study the thermal expansion or magnetostriction is the strain-gauge technique. It is based on a simple electrical resistance measurement. A resistive strain gauge consists ideally of a meander-type resistance structure to enhance the sensitivity. The strain gauge is glued directly on the sample. The expansion, respectively, contraction of the sample gives a change in the length of the strain gauge, which is detectable in the electrical resistance of the strain gauge. This technique has a much better resolution than X-ray or neutron scattering [15], but it does by far not reach the sensitivity of a capacitive dilatometer used at ambient pressure [94]. The limited sensitivity restricts the use of this probe under pressure primarily to the detection of structural phase transitions. X-ray and neutron diffraction experiments can be conducted to pressures above 50 GPa using DAC's. The strain-gauge technique has been adapted to piston-cylinder type pressure cells [91, 92] and toroidal-anvil cells allowing to reach pressures up to 8 GPa [15].

6.4.5 Magnetic Susceptibility and Magnetization

The experimental setups for magnetic susceptibility (χ_{ac}) and magnetization (M) measurements under pressure can be divided in two groups: (i) experiments in which the whole pressure cell including the sample is measured in a conventional magnetometer or susceptometer [97–100], e.g. a commercial SQUID magnetometer and (ii) setups where the sample is placed in a susceptometer which resides inside the pressure cell. The first measurement procedure has the disadvantage of a very small filling factor. In the second type of experimental setup the filling factor can be enhanced by

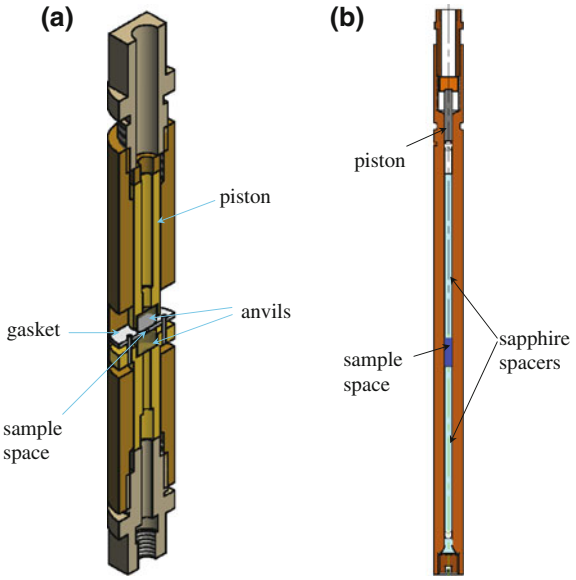

Fig. 6.9 **a** Schematic drawing of a DAC (after [95]) and **b** of a piston-cylinder type pressure cell [96] for a SQUID magnetometer

placing the susceptometer completely or at least its detection coil inside the high-pressure chamber [26, 33, 101–103].

There are several experimental setups belonging to the first group. For measurements in a commercial SQUID magnetometer the whole pressure cell is moved through the detection-coil system. Therefore, it is essential that the pressure cell is nonmagnetic and constructed as homogenous as possible. Ideally only the signal of the sample would be recorded. However, in reality this is not the case. In order to determine the magnetic properties of the sample, the background signal of the pressure cell without sample has to be determined and subtracted from the signal of the pressure cell with sample. Figure 6.9 shows two pressure cells for use in a commercial SQUID system. The DAC is capable of pressures up to 10 GPa [95] and the piston-cylinder type cell reaches about 1.4 GPa [96, 99]. The DAC provides only a very small sample space limiting the resolution of such a setup considerably. In a commercial SQUID magnetometer, e.g. the MPMS from Quantum Design, the lowest achievable temperature is only about 1.8 K and the magnetic field is limited to 7 T. Magnetization studies at lower temperatures and higher magnetic fields are possible with a capacitive Faraday magnetometer in a dilution refrigerator. Using a miniature piston-cylinder type pressure cell in this setup magnetization measurements can be carried out in the millikelvin range and in magnetic fields $B \lesssim 20$ T at pressures up to 1.5 GPa [104]. With the same pressure cell also specific-heat measurements are possible (see Fig. 6.8a and Sect. 6.4.3).

The actual design of the second type of experimental setups depends strongly on the type of pressure cell used and the available space in the sample chamber.

The susceptometer, a coil system, is composed of an excitation (primary) coil and a compensated detection (secondary) coil. The compensated coil consists of two parts wound in opposite direction in order to get a zero signal without sample. At ambient pressure the sample can be moved and measured in both parts of the compensated detection coil. In this way contributions coming from a non-ideal detection coil can be eliminated. This is not possible in pressure experiments. Here, the sample sits always in one part of the compensated detection coil. In piston-cylinder type pressure cells the whole coil system can be placed inside the pressure chamber [101, 103]. So much space is not available in opposed-anvil cells. In recent experimental realizations for opposed-anvil cells one part of the detection coil is placed inside the pressure chamber, while the second part, for the compensation, is placed outside [33, 102]. In earlier setups the whole coil system was fixed outside of the pressure chamber, directly on the anvils in order to obtain an as high as possible filling factor (e.g. [105]).

6.4.6 De Haas–van Alphen Oscillations

The measurement of de Haas–van Alphen oscillations (dHvA) is a powerful tool to study the metallic state. Together with band-structure calculations the Fermi-surface topology can be mapped out. At ambient pressure different methods are available to study dHvA oscillations. For measurements under pressure the field modulation technique is the only one which can be realized [106, 107]. The experimental setup is quite similar to that used for magnetic susceptibility measurements (see Sect. 6.4.5). The excitation coil is usually placed outside of the pressure cell and, to obtain a higher resolution, a compensated detection coil with the sample inside is placed in the pressure chamber. Since dHvA oscillations are typically only visible at very low temperatures and high magnetic fields a dilution refrigerator with a superconducting magnet capable of high magnetic fields is needed. Both, sweeping of the external field for measuring the dHvA oscillations and the modulation of the driving field, can lead to heating effects due to eddy currents induced in the pressure cell. While the former effect can be reduced by choosing a smaller sweeping rate at the expense of a longer duration of the experiment, a reduction of the amplitude of the modulation field reduces the sensitivity. Most of the dHvA experiments under pressure are carried out in the pressure range up to 3 GPa using piston-cylinder type pressure cells [106–109]. Recently, the feasibility to investigate dHvA oscillations at higher pressures has been demonstrated using a moissanite-anvil cell [110].

6.4.7 Magnetic Resonance

Magnetic resonance methods give access to local electronic and magnetic properties of strongly correlated materials, which are not accessible by the methods described above.

6.4.7.1 Nuclear Magnetic Resonance

The nuclear magnetic resonance (NMR) probes the local spin susceptibility at the site of the NMR nucleus and gives information on the local magnetic anisotropy. Furthermore, the spin-lattice relaxation rate can, for example, provide direct information on magnetic fluctuations. The experimental setup is related to the one for ac-susceptibility and dHvA experiments under pressure. A single detection coil as part of the NMR resonant circuit is placed inside the pressure chamber as described in Sect. 6.4.5. Broadband solid-state NMR experiments have been adapted to different types of pressure cells, like piston-cylinder type pressure cells, indenter type cells (see Fig. 6.5 which shows an NMR coil in the sample chamber) [26], opposed-anvil cells [111–113], and cubic-anvil type pressure cells [114].

6.4.7.2 Electron-Spin Resonance

In metallic systems usually an appropriate element (ESR-probe), e.g. Mn or Gd, which does not possess any orbital momentum, has to be doped into the compound under investigation to be able to measure the electron-spin resonance (ESR). ESR investigations under pressure using a classical resonator setup were well established [115], but are generally not in use anymore. With these setups pressures up to 3 GPa and above could be obtained. Only recently the discovery of an ESR signal in the heavy-fermion material $YbRh_2Si_2$ without any ESR probe [116] motivated a renewed interest in ESR measurements under pressure [117]. In addition to the classical ESR experiments, setups for high-field (high-frequency) ESR experiments under pressure have been developed and are used for investigations on quantum-spin systems [118–120].

6.4.7.3 Muon-Spin Rotation/Resonance

μSR stands for both muon-spin rotation and muon-spin resonance. The acronym already draws the attention to the analogy with ESR and NMR. The muons are implanted in the sample and decay after 2.2 μs as $\mu^+ \rightarrow e^+ + \nu_\mu + \nu_e$. The angular distribution of e^+ has a maximum in the muon spin direction. The muon spins precess in a transverse magnetic field, which is equivalent to the free induction decay in pulsed NMR. This is called muon-spin rotation (TF-μSR) in contrast to the muon-spin resonance (RF-μSR). Here, the muon-spin polarization is along the magnetic field and transitions are induced by an RF-field as in conventional NMR. μSR can detect extremely small internal fields. Furthermore, magnetic fluctuations in the range 10^4–10^{12} Hz can be investigated. A comprehensive review on heavy-fermion systems and type-II superconductors studied by μSR techniques can be found in [121] and [122, 123] respectively.

For μSR experiments under pressure a large sample size is essential to obtain a good signal-to-background ratio. Thus, only piston-cylinder type pressure cells are

suitable for μSR measurements under pressure. This limits the achievable pressure to about 3 GPa. Pressure experiments can be carried out at temperatures down to 0.25 K using ^{3}He cryostats (see [124, 125] as an example of a recent study).

6.4.8 Neutron Scattering

Neutron-scattering experiments allow the study of different physical properties. Neutron diffraction is an important tool to investigate crystal (see Sect. 6.4.4) and magnetic structures. Inelastic neutron scattering provides information on different types of excitations. These can include magnetic excitations, which are of special interest in the field of correlated matter, but also crystal-electric field (CEF) and phonon excitations [126].

The biggest challenge for neutron-scattering experiments under pressure is to reduce the additional background signal due to the pressure cell. Crystal-structure investigations need only a relatively small sample size. Using anvil cells pressures up to 50 GPa can be achieved (see for example [127–132]). The investigation of magnetic structures is more challenging due to the low intensity of the magnetic reflections, especially in materials with small magnetic moments. Usually piston-cylinder type cells are utilized in neutron-scattering investigations of magnetic properties under pressure because of their large volume available for the sample [133–137]. A comprehensive introduction to neutron scattering techniques in high-pressure environments can be found in [138].

6.4.9 Mössbauer Spectroscopy

Mössbauer spectroscopy is an effective microscopic tool to investigate magnetic moments and magnetic ordering phenomena. It also reveals the electric-field gradient (EFG) at the site of the Mössbauer active nucleus. Unfortunately, only a very limited number of Mössbauer active nuclei exist. In heavy-fermion materials Mössbauer investigations under pressure have been conducted in Yb-based compounds using ^{170}Yb as Mössbauer active nucleus ([139] and references therein). Mössbauer spectroscopy is also possible on ^{238}U and ^{151}Eu, but no pressure studies are reported. In the iron-based superconductors ^{57}Fe is a Mössbauer active nucleus which allows Mössbauer investigations under pressure directly at the magnetic site (e.g. [140]). Using DAC's Mössbauer experiments can be carried out at cryogenic temperatures at pressures up to 100 GPa [139, 141–143].

6.4.10 Optical Spectroscopy and Related Techniques

Raman scattering, Brillouin scattering, and optical/X-ray spectroscopy are important tools to investigate the effects of electron-phonon coupling and electronic correlations in materials like high-temperature superconductors or transition-metal oxides. Since these techniques require an optical access to the sample, DAC's are regularly utilized. For further details on pressure experiments with these probes we refer to the literature (see for example [144–147] and references therein).

6.5 Pressure Tuning of Strongly Correlated Materials

External pressure has been successfully used to study different classes of strongly correlated materials, like low-dimensional organic conductors (for example [148, 149] and references therein), the recently discovered iron-based superconductors (for example [150] and references therein), or the heavy-fermion materials. In the following we will demonstrate the importance of pressure studies for the understanding of heavy-fermion supeconductors on some selected examples.

$CeCu_2Si_2$, the first heavy-fermion superconductor [151], shows a very broad superconducting region under pressure [152]. Even though this unusual superconducting regime was reported already short after the discovery of $CeCu_2Si_2$ its origin remained puzzling for many years. It was speculated that the low-pressure superconducting region is related to the proximity to antiferromagnetism and that in the high-pressure region valence fluctuations might play an important role [152–154]. A combined pressure and substitution experiment could finally show that indeed two distinct superconducting regions exist in $CeCu_2Si_2$ [155].

Pressure investigations have been highly successful in the discovery of new unconventional Ce-based heavy-fermion superconductors. The heavy-fermion antiferromagnet $CeCu_2Ge_2$ is isoelectronic to $CeCu_2Si_2$, but has a larger unit-cell volume. It was therefore a natural step to apply pressure on $CeCu_2Ge_2$ in order to reduce its unit-cell volume to that of $CeCu_2Si_2$ and look for superconductivity. Application of pressure indeed suppresses the magnetic order and an extended superconducting phase develops above 7.5 GPa [156]. In this way $CeCu_2Ge_2$ was not a completely new heavy-fermion superconductor, since its pressure dependence reproduces that of $CeCu_2Si_2$. Nevertheless, the experimental concept to use pressure to suppress the antiferromagnetic state to induce superconductivity led to the discovery of many Ce-based heavy-fermion pressure-induced superconductors, e.g. $CeRh_2Si_2$ [157], $CePd_2Si_2$ [158], or $CeIn_3$ [158, 159]. Figure 6.10 displays the $T-p$ phase diagram of $CeIn_3$ which is also representative for that of $CeRh_2Si_2$ and $CePd_2Si_2$. In these and several other Ce-based heavy-fermion materials superconductivity develops around the critical pressure where the antiferromagnetic order is suppressed, suggesting that the superconductivity is magnetically mediated.

In the following we will highlight how pressure studies contributed to the understanding of the $CeMIn_5$ heavy-fermion materials (M = Co, Rh, and Ir).

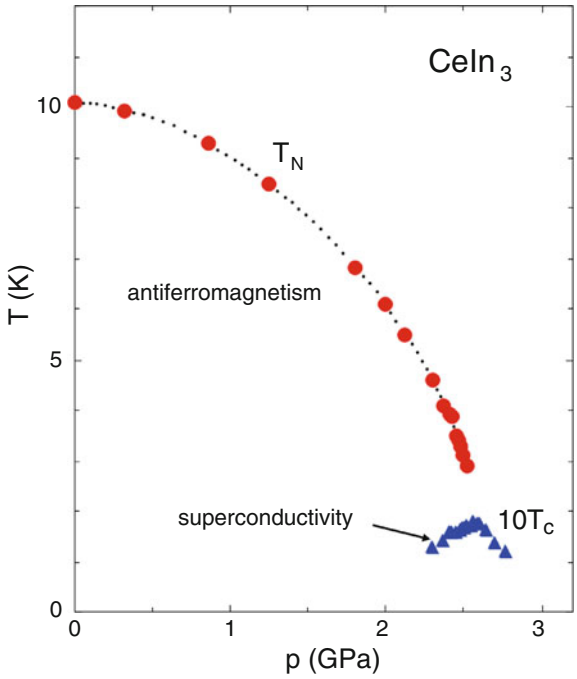

Fig. 6.10 $T-p$ phase diagram of $CeIn_3$. The data were taken from [158]

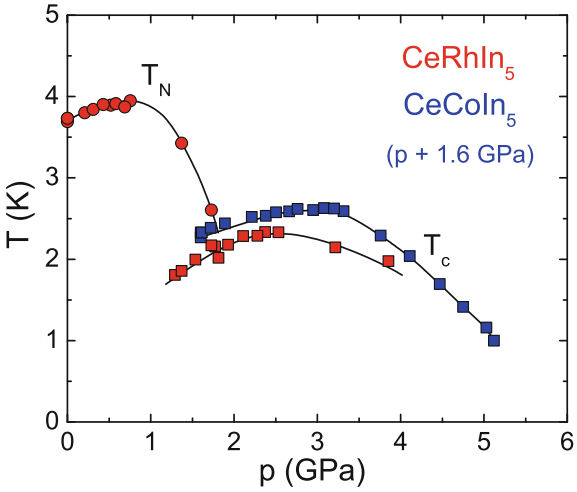

Fig. 6.11 Combined $T-p$ phase diagram of $CeRhIn_5$ and $CeCoIn_5$. The data of $CeCoIn_5$ have been shifted by 1.6 GPa. The data were taken from [161–164]

The CeMIn$_5$ compounds are layered materials which consist of layers of CeIn$_3$ separated by layers of MIn$_2$ [160]. Therefore, CeIn$_3$ can be considered the parent compound of the CeMIn$_5$ family. At ambient pressure CeIn$_3$ orders antiferromagnetically below $T_N \approx 10$ K. Application of pressure suppresses T_N to zero temperature at $p_c \approx 2.5$ GPa [158]. Around p_c superconductivity develops below $T_c \approx 200$ mK (see also Fig. 6.10).

CeRhIn$_5$ orders antiferromagnetically like CeIn$_3$, but has a considerably lower $T_N = 3.8$ K [165]. On application of pressure the antiferromagnetic order is suppressed around 1.9 GPa and superconductivity starts to develop [165]. A broad superconducting dome with a maximum T_c of 2.3 K extends over more than 4 GPa in the T–p phase diagram [161, 163, 165]. While the phase diagram of CeRhIn$_5$ is reminiscent of that of other heavy-fermion superconductors, it shows one important difference, the antiferromagnetic and superconducting ordering temperatures are of the same order. CeCoIn$_5$ and CeIrIn$_5$ are ambient pressure superconductors with $T_c = 2.3$ K [166] and 0.4 K [167], respectively. Detailed experiments confirm the unconventional nature of the superconductivity [168]. The T–p phase diagram of CeCoIn$_5$ displays a broad superconducting dome which extends up to 5 GPa similar to CeRhIn$_5$ [162, 164]. An estimation using the experimental bulk modulus and lattice parameters of CeCoIn$_5$ and CeRhIn$_5$ suggests that CeCoIn$_5$ is under an effective pressure of 1.6 GPa compared with CeRhIn$_5$. Shifting the phase diagram of CeCoIn$_5$ by this value and superimposing it on that of CeRhIn$_5$ leads indeed to a good agreement between the two phase diagrams (see Fig. 6.11). This suggests that at ambient pressure CeCoIn$_5$ is situated in close proximity to antiferromagnetic order.

This finding is supported by studies on Cd substituted CeCoIn$_5$, where In was replaced by a small amount of Cd [169]. For substitution levels of more than $x \approx 0.075$ antiferromagnetism is induced in CeCo(In$_{1-x}$Cd$_x$)$_5$ [169]. In the concentration range $0.075 \lesssim x \lesssim 0.0125$ superconductivity coexists with the antiferromagnetic order at low temperatures [169–171]. Pressure studies on the substituted compounds revealed a T–p phase diagram which can be superimposed on that of CeRhIn$_5$ and CeCoIn$_5$, shown in Fig. 6.11, by considering an appropriate pressure shift [169]. However, there is no direct correspondence of the unit-cell volumes of the different compounds.

CeIrIn$_5$ is the second ambient pressure superconductor in the CeMIn$_5$ family. The superconducting transition temperature of only $T_c = 0.4$ K is rather small compared with the T_c of CeCoIn$_5$ [166, 167]. $T_c(p)$ exhibits also a dome-like shape with a maximum $T_c \approx 1$ K at about 2.5 GPa [173]. In contrast to CeCoIn$_5$ there are no obvious candidates for the superconducting coupling mechanism.

Substituting Rh by Ir in CeRh$_{1-x}$Ir$_x$In$_5$ suppresses the antiferromagnetic order at a critical concentration of about $x_c = 0.65$ (see Fig. 6.12) [174]. A broad superconducting phase covers the $T - x$ phase diagram starting from $x = 0.35$ up to CeIrIn$_5$ [174]. On a first look this might suggest that the superconductivity in CeIrIn$_5$ is related to the pressure-induced superconducting phase in CeRhIn$_5$, similar like in CeCoIn$_5$. However, there is a small dip in $T_c(x)$ around $x = 0.9$ [174]. The dip was taken as a hint for the existence of two distinct superconducting phases in the phase diagram of CeRh$_{1-x}$Ir$_x$In$_5$ [172, 174]. This would imply that the superconductivity in CeIrIn$_5$

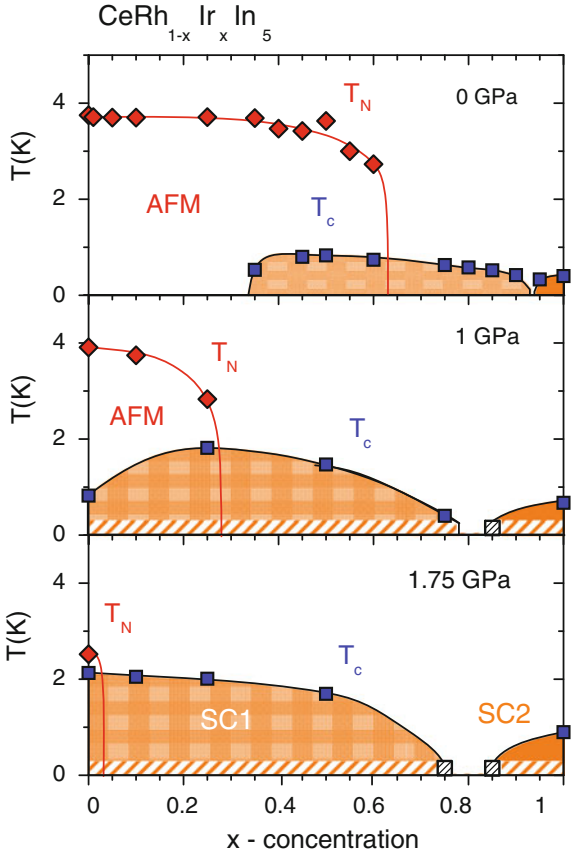

Fig. 6.12 T–x phase diagram of $CeRh_{1-x}Ir_xIn_5$ at ambient pressure, 1 GPa, and 1.75 GPa. The phase diagram evidences the existence of two distinct superconducting phases, SC1 and SC2. The data were taken from [172]

is disconnected from that in $CeRhIn_5$ and, therefore, possibly different in origin. A combined doping and pressure study answered the question and showed that two separated superconducting phases exist in $CeRh_{1-x}Ir_xIn_5$ [172]. The application of pressure slowly removes the antiferromagnetism from the $T - x$ phase diagram. At 1 GPa the critical concentration is only $x_c \approx 0.35$ compared to $x_c \approx 0.65$ at ambient pressure. Finally, at 1.75 GPa only $CeRhIn_5$ exhibits antiferromagnetic order (see Fig. 6.12) [172]. While the antiferromagnetic region becomes narrower upon increasing pressure, the dip in $T_c(x)$ evolves into a range without superconductivity. This result evidences that two distinct superconducting phases, SC1 and SC2, exist in $CeRh_{1-x}Ir_xIn_5$. The position of the maximum of the superconducting dome SC1 is correlated with the critical concentration, x_c, for the disappearance of the antiferromagnetic order. This hints at a magnetic coupling mechanism in the super-

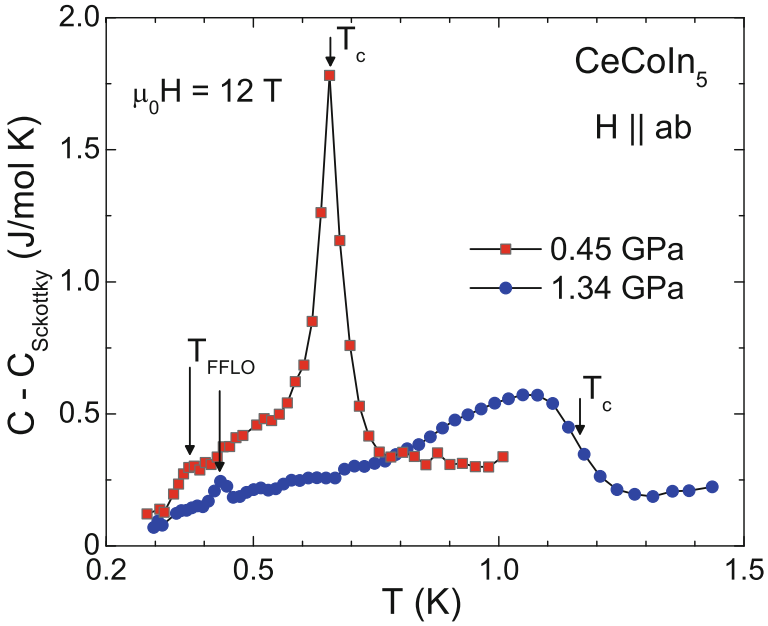

Fig. 6.13 Low-temperature specific heat of $CeCoIn_5$ at 0.45 GPa and 1.34 GPa in a magnetic field of 12 T applied in the *ab* plane. The specific heat at both pressures shows two phase transitions, which are marked by *arrows*. The experiment was carried out using the pressure cell shown in Fig. 6.8b. The data were taken from [76]

conducting phase SC1. The superconducting phase SC2 is disconnected from any magnetic order, thus leaving open the question about the superconducting pairing mechanism in $CeIrIn_5$ [172].

There are more peculiar findings in the $CeMIn_5$ materials. $CeCoIn_5$ shows a second phase-transition anomaly inside the superconducting state close to the upper critical field, $H_{c2}(0)$, for $H \| ab$ [175, 176]. This unusual observation was taken as a strong hint at the realization of the Fulde-Ferrell-Larkin-Ovchinnikov (FFLO) superconducting state [177, 178]. $CeCoIn_5$ does not only show this anomaly, but also fulfills the pre-conditions for the formation of such a state. The FFLO state is an inhomogeneous superconducting state due to competition between superconductivity and Pauli paramagnetism, which had been proposed already in the 1960s [177, 178].

Even though there is strong evidence for the realization of the FFLO phase in $CeCoIn_5$, there remains also the possibility that this phase is magnetic in origin. We have shown before that $CeCoIn_5$ is situated close to a magnetic instability. Furthermore, the observed non-Fermi liquid behavior in thermodynamic and transport properties evidences the presence of strong magnetic fluctuations [166]. Application of external pressure enables us to move $CeCoIn_5$ away from these magnetic fluctuations. Electrical-resistivity and Hall-effect studies under pressure evidence that the mag-

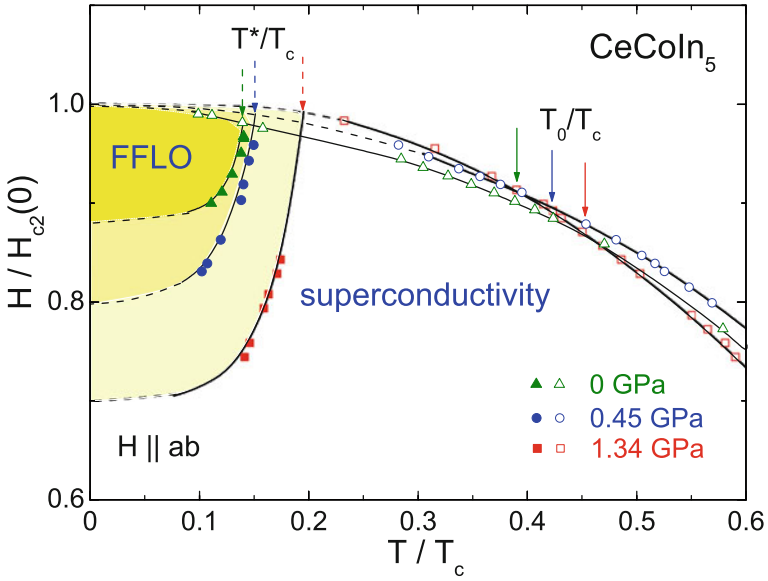

Fig. 6.14 Magnetic field—temperature phase diagram of $CeCoIn_5$ at different pressures. The phase diagram shows the evolution of the low-temperature phase inside the superconducting state. The axes are normalized by the upper-critical field $H_{c2}(0)$ and the superconducting transition temperature T_c, respectively. The data were taken from [76]

netic fluctuations in $CeCoIn_5$ are effectively suppressed around 1.5 GPa [179, 180]. Therefore, a study of the effect of pressure on the low-temperature phase inside the superconducting state in $CeCoIn_5$ can help to clarify the nature of this unusual phase.

Figure 6.13 shows specific-heat data recorded at 12 T at 0.45 and 1.34 GPa [181]. At both pressures the anomaly at the transition into the superconducting state and an additional anomaly inside the superconducting phase are clearly visible. At 12 T the shape of the anomaly at T_c is qualitatively different at 0.45 GPa and 1.34 GPa. At 0.45 GPa it indicates a first-order type phase transition, while at 1.34 GPa the shape of the anomaly is typical for a second-order type transition. At 1.34 GPa the character of the phase transition changes from second- to first-order slightly above 12 T [181, 182]. We note that upon increasing pressure both transitions shift to higher temperatures. The phase diagram in Fig. 6.14 summarizes the results from the specific-heat experiments. The field axis is normalized by the corresponding upper-critical field at zero temperature, $H_{c2}(0)$, and the temperature by T_c at zero field. The low-temperature phase in the superconducting state expands upon increasing pressure. This is generally not expected, if the low-temperature phase would be purely magnetic in nature, since pressure favors a non-magnetic state in Ce-based heavy-fermion metals. Therefore, the pressure studies are in support of a realization of the FFLO state in $CeCoIn_5$. However, neutron scattering experiments find a small field induced magnetic moment at an incommensurate wave-vector inside the low-temperature phase which is not compatible with the FFLO state [183]. The real nature of this phase is still under debate. Several theoretical models have been proposed

to account for this so-far unique relationship between magnetism and superconductivity. Studies of microscopic properties under pressure, e.g. by NMR or by neutron scattering, could help to reveal the true nature of this unusual phase in $CeCoIn_5$.

These examples show that pressure studies do not only contribute to the general understanding of strongly correlated materials. They can lead to the discovery of new unconventional phases or help to answer specific physical questions.

Acknowledgments I would like to thank C. Klausnitzer for the careful preparation of the illustrations. Furthermore, I am indebted to K. Mydeen and E. Lengyel for valuable comments on the manuscript.

References

1. M.I. Eremets, *High Pressure Extperimental Methods* (Oxfrord University Press, Oxford, 1996)
2. T. Matsumoto, Rev. High Press. Sci. Techn. **12**, 280 (2002). doi:10.4131/jshpreview.12.280
3. I.R. Walker, Rev. Sci. Instrum. **70**, 3402 (1999). doi:10.1063/1.1149927
4. Y. Uwatoko, S. Todo, K. Ueda, A. Uchida, M. Kosaka, N. Mori, T. Matsumoto, J. Phys.: Condens. Matter **14**, 11291 (2002). doi:10.1088/0953-89844/44/469
5. Y. Uwatoko, M. Hedo, N. Kurita, M. Kodea, M. Abliz, T. Matsumoto, Phys. B **329—-333**, 1658 (2003). doi:10.1016/s0921-4526(02)02449-3
6. H. Taniguchi, S. Takeda, R. Satoh, A. Taniguchi, H. Komatsu, K. Satoh, Rev. Sci. Instrum. **81**, 033903 (2010). doi:10.1063/1.3310197
7. C. Pfleiderer, E. Bedin, B. Salce, Rev. Sci. Instrum. **68**, 3120 (1997). doi:10.1063/1.1148254
8. B. Salce, J. Thomasson, A. Demuer, J.J. Blanchard, J.M. Martinod, L. Devoille, A. Guillaume, Rev. Sci. Instrum. **71**, 2461 (2000). doi:10.1063/1.1150664
9. M. Nicklas, (2007). Unpublished
10. T. Nakanishi, Rev. High Press. Sci. Techn. **11**, 187 (2001). doi:10.4131/jshpreview.11.187
11. T. Nakanishi, N. Takeshita, N. Mori, Rev. Sci. Instrum. **73**, 1828 (2002). doi:10.1063/1.1458044
12. T. Nakanishi, M. Nicklas, G. Sparn, F. Steglich, J. Phys. Soc. Jpn. **76SA**, 223 (2007). doi:10.1143/JPSJS.76SA.223
13. A.S. Rüetschi, D. Jaccard, Rev. Sci. Instrum. **78**, 123901 (2007). doi:10.1063/1.2818788
14. E. Colombier, D. Braithwaite, Rev. Sci. Instrum. **78**, 1 (2007). doi:10.1063/1.2778629
15. O.B. Tsiok, V.V. Bredikhin, V.A. Sidorov, L.G. Khvostantsev, High Press. Res. **10**, 523 (1992). doi:10.1080/08957959208201471
16. L.G. Khvostantsev, V.A. Sidorov, O.B. Tsiok, High pressure toroid cell: Applications in planetary and material sciences. Geophys. Monogr. Ser. **101**, 89 (1998)
17. A.E. Petrova, V.A. Sidorov, S.M. Stishov, Physica B **359—-361**, 1463 (2005). doi:10.1016/j.physb.2005.01.454
18. W.A. Bassett, High Press. Res. **29**, 163 (2009). doi:10.1080/08957950802597239
19. A. Jayaraman, Rev. Mod. Phys **55**, 65 (1983). doi:10.1103/RevModPhys.55.65
20. D.J. Dunstan, I.L. Spain, J. Phys. E: Sci. Instrum. **22**, 913 (1989). doi:10.1088/0022-3735/221/004
21. I.L. Spain, D.J. Dunstan, J. Phys. E: Sci. Instrum. **22**, 923 (1989). doi:10.1088/0022-3735/221/005
22. G.Y. Machavariani, M.P. Pasternak, G.R. Hearne, Rev. Sci. Instrum. **69**, 1423 (1998). doi:10.1063/1.1148775
23. M. Kano, N. Kurita, M. Hedo, Y. Uwatoko, S.W. Tozer, H.S. Suzuki, T. Onimaru, T. Sakakibara, J. Phys. Soc. Jpn. **76SA**, 56 (2007). doi:10.1143/JPSJS.76SA.56

24. A.G. Gavriliuk, A.A. Mironovich, V.V. Struzhkin, Rev. Sci. Instrum. **80**, 043906 (2009). doi:10.1063/1.3122051
25. G. Giriat, W. Wang, J.P. Attfield, A.D. Huxley, K.V. Kamenev, Rev. Sci. Instrum. **81**, 073905 (2010). doi:10.1063/1.3465311
26. T.C. Kobayashi, H. Hidaka, T. Fujiwara, M. Tanaka, K. Takeda, T. Akazawa, K. Shimizu, S. Kirita, R. Asai, H. Nakawaki, M. Nakashima, R. Settai, Y. Yamamoto, Y. Haga, Y. Ōnuki, J. Phys.: Condens. Matter **19**, 125205 (2007). doi:10.1088/0953-8984/19/12/125205
27. N. Mori, H. Takahashi, N. Takeshita, High Press. Res. **24**, 225 (2004). doi:10.1080/08957950410001661909
28. Y. Uwatoko, K. Matsubayashi, T. Matsumoto, N. Aso, M. Nishi, T. Fujiwara, M. Hedo, S. Tabata, K. Takagi, M. Tado, H. Kagi, Rev. High Press. Sci. Techn. **18**, 230 (2008). doi:10.4131/jshpreview.18.230
29. T. Hikita, T. Maruyama, N. Yamada, Jpn. J. Appl. Phys. **29**, 2519 (1990). doi:10.1143/jjap.29.2519
30. S.M. Stishov, A.E. Petrova, J. Phys. Soc. Jpn. **76SA**, 212 (2007). doi:10.1143/JPSJS.76SA.212
31. O.P. Welzel, F.M. Grosche, Rev. Sci. Instrum. **82**, 033901 (2011). doi:10.1063/1.3541793
32. S.T. Weir, J. Akella, C. Aracne-Ruddle, Y.K. Vohra, S.A. Catledge, Appl. Phys. Lett. **77**, 3400 (2000). doi:10.1063/1.1326838
33. D.D. Jackson, C. Aracne-Ruddle, V. Malba, S.T. Weir, S.A. Catledge, Y.K. Vohra, Rev. Sci. Instrum. **74**, 2467 (2003). doi:10.1063/1.1544084
34. X. Ji-an, M. Ho-kwang, R.J. Hemley, E. Hines, J. Phys.: Condens. Matter **14**, 11543 (2002). doi:10.1088/0953-89844/44/513
35. J.D. Thompson, Rev. Sci. Instrum. **55**, 231 (1984). doi:10.1063/1.1137730
36. O.E. Andersson, B. Sundqvist, Rev. Sci. Instrum. **68**, 1344 (1997). doi:10.1063/1.1147868
37. L.H. Dmowski, E. Litwin-Staszewska, Meas. Sci. Technol. **10**, 343 (1999). doi:10.1088/0957-02330/5/001
38. L.H. Dmowski, J. Przybytek, E. Litwin-Staszewska, High Press. Res. **19**, 743 (2000). doi:10.1080/08957950008202577
39. F.P. Bundy, Phys. Rev. **110**, 314 (1958). doi:10.1103/PhysRev.110.314
40. G. Andersson, B. Sundqvist, G. Bäckström, J. Appl. Phys. **65**, 3943 (1989). doi:10.1063/1.343360
41. A. Eiling, J.S. Schilling, J. Phys. F: Met. Phys. **623**, 11 (1981). doi:10.1088/0305-46081/3/010
42. B. Bireckoven, J. Wittig, J. Phys. E: Sci. Instrum. **21**, 841 (1988). doi:10.1088/0022-3735/21/9/004
43. J.D. Barnett, S. Block, G.J. Piermarini, Rev. Sci. Instrum. **44**, 1 (1973). doi:10.1063/1.1685943
44. G.J. Piermarini, S. Block, Rev. Sci. Instrum. **46**, 973 (1975). doi:10.1063/1.1134381
45. H.K. Mao, J. Xu, P.M. Bell, J. Geophys. Res. **91**, 4673 (1986). doi:10.1029/JB091iB05p04673
46. R.J. Hemley, C.S. Zha, A.P. Jephcoat, H.K. Mao, L.W. Finger, D.E. Cox, Phys. Rev. B **39**, 11820 (1989). doi:10.1103/PhysRevB.39.11820
47. D.D. Ragan, R. Gustavsen, D. Schiferl, J. Appl. Phys. **72**, 5539 (1992). doi:10.1063/1.351951
48. A.P. Reyes, E.T. Ahrens, R.H. Heffner, P.C. Hammel, J.D. Thompson, Rev. Sci. Instrum. **63**, 3120 (1992). doi:10.1063/1.1142564
49. H. Fukazawa, N. Yamatoji, Y. Kohori, C. Terakura, N. Takeshita, Y. Tokura, H. Takagi, Rev. Sci. Instrum. **78**, 015106 (2007). doi:10.1063/1.2426875
50. D.L. Decker, T.G. Worlton, J. Appl. Phys. **43**, 4799 (1972). doi:10.1063/1.1661013
51. w Yu, A.A. Aczel, T.J. Williams, S.L. Budko, N. Ni, P.C. Canfield, G.M. Luke, Phys. Rev. B **79**, 020511 (2009). doi:10.1103/PhysRevB.79.020511
52. N. Tateiwa, S. Ikeda, Y. Haga, T.D. Matsuda, M. Nakashima, D. Aoki, R. Settai, Y. Ōnuki, J. Phys.: Conf. Ser **150**, 042206 (2009). doi:10.1088/1742-6596/150/4/042206
53. D.D. Ragan, D.R. Clarke, D. Schiferl, Rev. Sci. Instrum. **67**, 494 (1996). doi:10.1063/1.1146627

54. T. Varga, A.P. Wilkinson, R.J. Angel, Rev. Sci. Instrum. **74**, 4564 (2003). doi:10.1063/1.1611993
55. Y. Shen, R.S. Kumar, M. Pravica, M.F. Nicol, Rev. Sci. Instrum. **75**, 4450 (2004). doi:10.1063/1.1786355
56. V.A. Sidorov, R.A. Sadykov, J. Phys.: Condens. Matter **17**, S3005 (2005). doi:10.1088/0953-8984/17/40/002
57. A.S. Kirichenko, A.V. Kornilov, V.M. Pudalov, Instrum. Exp. Tech. **48**, 813 (2005). doi:10.1007/s10786-005-0144-5
58. K. Yokogawa, K. Murata, H. Yoshino, S. Aoyama, Jpn. J. Appl. Phys. **46**, 3636 (2007). doi:10.1143/JJAP.46.3636
59. K. Murata, K. Yokogawa, H. Yoshino, S. Klotz, P. Munsch, A. Irizawa, M. Nishiyama, K. Iizuka, T. Nanba, T. Okada, Y. Shiraga, S. Aoyama, Rev. Sci. Instrum. **79**, 085101 (2008). doi:10.1063/1.2964117
60. S. Klotz, J.C. Chervin, P. Munsch, G.L. Marchand, J. Phys. D: Appl. Phys. **42**, 075413 (2009). doi:10.1088/0022-3727/42/7/075413
61. S. Klotz, L. Paumier, G.L. Marchand, P. Munsch, High Press. Res. **29**, 649 (2009). doi:10.1080/08957950903418194
62. Y. Feng, R. Jaramillo, J. Wang, Y. Ren, T.F. Rosenbaum, Rev. Sci. Instrum. **81**, 041301 (2010). doi:10.1063/1.3400212
63. E.S. Itskevich, V.F. Kraidenov, Cryogenics **15**, 552 (1975). doi:10.1016/0011-2275(75)90154-X
64. P. Andersson, G. Bäckström, Rev. Sci. Instrum. **47**, 205 (1976). doi:10.1063/1.1134581
65. S. Andersson, G. Bäckström, Rev. Sci. Instrum. **57**, 1633 (1986). doi:10.1063/1.1138542
66. G.F. Chen, I. Sakamoto, S. Ohara, T. Takami, H. Ikuta, U. Mizutani, Phys. Rev. B **69**, 14420 (2004). doi:10.1103/PhysRevB.69.014420
67. A.K. Singh, G. Ramani, Rev. Sci. Instrum. **49**, 1324 (1978). doi:10.1063/1.1135577
68. P.M. Chaikin, C. Weyl, G. Malfait, D. Jérome, Rev. Sci. Instrum. **52**, 1397 (1981). doi:10.1063/1.1136780
69. D. Jaccard, E. Vargoz, K. Alami-Yadri, H. Wilhelm, Rev. High Press. Sci. Techn. **7**, 412 (1998). doi:10.4131/jshpreview.7.412
70. H. Wilhelm, AC-calorimetry at high pressure and low temperature. Adv. in Solid State Phys. **43**, 889 (2003). doi:10.1007/978-3-540-44838-9_63
71. D. Jaccard, K. Sengupta, Rev. Sci. Instrum. **81**, 041301 (2010). doi:10.1063/1.3360819
72. D.A. Polvani, J.F. Meng, M. Hasegawa, J.V. Badding, Rev. Sci. Instrum. **70**, 3586 (1999). doi:10.1063/1.1149964
73. E.S. Choi, K. Haeyong, Y.J. Jo, W. Kang, Rev. Sci. Instrum. **73**, 2999 (2002). doi:10.1063/1.1489076
74. R. Borth, M. Nicklas, (2012). Unpublished.
75. C.F. Miclea, M. Nicklas, J.L. Sarrao, G. Sparn, F. Steglich, J.D. Thompson, AIP Conf. Proc. 850, 713 (2006). doi:10.1063/1.2354906
76. C.F. Miclea, M. Nicklas, J.L. Sarrao, G. Sparn, F. Steglich, J.D. Thompson, Phys. B **378–380**, 398 (2006). doi:10.1016/j.physb.2006.01.174
77. J.C. Ho, N.E. Phillips, T.F. Smith, Phys. Rev. Lett. **17**, 694 (1966). doi:10.1103/PhysRevLett.17.694
78. A. Berton, J. Chaussy, B. Cornut, J. Odin, J. Paureau, J. Peyrard, Cryogenics **19**, 543 (1979). doi:10.1016/0011-2275(79)90009-2
79. F. Tomioka, I. Umehara, T. Ono, M. Hedo, Y. Uwatoko, N. Kimura, Jpn. J. Appl. Phys. **46**, 3090 (2007). doi:10.1143/jjap.46.3090
80. H. Wilhelm, T. Lühmann, T. Rus, F. Steglich, Rev. Sci. Instrum. **75**, 2700 (2004). doi:10.1063/1.1771486
81. R. Bachmann, J.F.J. DiSalvo, T.H. Geballe, R.L. Greene, R.E. Howard, C.N. King, H.C. Kirsch, K.N. Lee, R.E. Schwall, H.U. Thomas, R.B. Zubeck, Rev. Sci. Instrum. **43**, 205 (1972). doi:10.1063/1.1685596
82. M. Brando, Rev. Sci. Instrum. **80**, 095112 (2009). doi:10.1063/1.3202380

83. P.F. Sullivan, G. Seidel, Phys. Rev. **173**, 679 (1968). doi:10.1103/PhysRev.173.679
84. E. Gmelin, Thermochim. Acta **305**, 1 (1997). doi:10.1016/S0040-6031(97)00126-3
85. A. Demuer, C. Marcenat, J. Thomasson, R. Calemczuk, B. Salce, P. Lejay, D. Braithwaite, J. Flouquet, J. Low Temp. Phys. **120**, 245 (2000). doi:10.1023/a:1004685711942
86. E.S. Itskevich, V.F. Kraidenov, Instrum. Exp. Tech. **21**, 1640 (1978)
87. A. Eichler, W. Gey, Rev. Sci. Instrum. **50**, 1445 (1979). doi:10.1063/1.1135737
88. F. Bouquet, Y. Wang, H. Wilhelm, D. Jaccard, A. Junod, Solid State Commun. **113**, 367 (2000). doi:10.1016/s0038-1098(99)00505-0
89. H. Wilhelm, D. Jaccard, J. Phys.: Condens. Matter **14**, 10683 (2002). doi:10.1088/0953-89844/44/357
90. K. Matsubayashi, M. Hedo, I. Umehara, N. Katayama, K. Ohgushi, A. Yamada, K. Munakata, T. Matsumoto, Y. Uwatoko, J. Phys.: Conf. Ser. **215**, 012187 (2010). doi:10.1088/1742-6596/215/1/012187
91. G. Oomi, T. Kagayama, Y. Ōnuki, T. Komatsubara, Phys. B **163**, 557 (1990). doi:10.1016/0921-4526(90)90268-Y
92. G. Oomi, T. Kagayama, Phys. B **201**, 235 (1994). doi:10.1016/0921-4526(94)91090-1
93. R.S. Kumar, A.L. Cornelius, J.L. Sarrao, Phys. Rev. B **70**, 214526 (2004). doi:10.1103/PhysRevB.70.214526
94. R. Küchler, T. Bauer, M. Brando, F. Steglich, Rev. Sci. Instrum. **83**, 095102 (2012). doi:10.1063/1.4748864
95. P.L. Alireza, G.G. Lonzarich, Rev. Sci. Instrum. **80**, 023906 (2009). doi:10.1063/1.3077303
96. M. Nicklas, (2009). Unpublished.
97. D. Wohlleben, M.B. Maple, Rev. Sci. Instrum. **42**, 1573 (1971). doi:10.1063/1.1684942
98. K. Koyama, S. Hane, K. Kamishima, T. Goto, Rev. Sci. Instrum. **69**, 3009 (1998). doi:10.1063/1.1149048
99. K.V. Kamenev, S. Tancharakorn, A. Robertson, A. Harrison, Rev. Sci. Instrum. **77**, 73905 (2006). doi:10.1063/1.2221537
100. P.L. Alireza, S. Barakat, A.M. Cumberlidge, G. Lonzarich, F. Nakamura, J. Phys. Soc. Jpn. **76SA**, 216 (2007). doi:10.1143/JPSJS.76SA.216
101. C. Pfleiderer, Rev. Sci. Instrum. **68**, 1532 (1997). doi:10.1063/1.1147642
102. P.L. Alireza, S.R. Julian, Rev. Sci. Instrum. **74**, 4728 (2003). doi:10.1063/1.1614861
103. M. Ohashi, G. Oomi, J. Phys. Soc. Jpn. **76SA**, 226 (2007). doi:10.1143/JPSJS.76SA.226
104. Y. Tokiwa, P. Gegenwart, T. Radu, J. Ferstl, G. Sparn, C. Geibel, F. Steglich, Phys. Rev. Lett. **94**, 226402 (2005). doi:10.1103/PhysRevLett.94.226402
105. C.C. Kim, M.E. Reeves, M.S. Osofsky, E.F. Skelton, D.H. Liebenberg, Rev. Sci. Instrum. **65**, 992 (1994). doi:10.1063/1.1144878
106. M. Takashita, H. Aoki, T. Matsumoto, C.J. Haworth, T. Terashima, A. Uesawa, T. Suzuki, Phys. Rev. Lett. **78**, 1948 (1997). doi:10.1103/PhysRevLett.78.1948
107. M.S. Nam, J. Singleton, A.K. Klehe, W. Hayes, M. Kurmoo, P. Day, Synth. Met. **103**, 2259 (1999). doi:10.1016/s0379-6779(98)00444-5
108. H. Shishido, R. Settai, D. Aoki, S. Ikeda, H. Nakawaki, N. Nakamura, T. Iizuka, Y. Inada, K. Sugiyama, T. Takeuchi, K. Kindo, C. Kobayashi, Y. Haga, H. Harima, Y. Aoki, T. Namiki, H. Sato, Y. Ōnuki, Phys. Soc. Jpn. **71**, 162 (2002). doi:10.1143/jpsj.71.162
109. Y. Ōnuki, R. Settai, Low Temp. Phys. **38**, 89 (2012). doi:10.1063/1.3683408
110. S.K. Goh, P.L. Alireza, P.D.A. Mann, A.M. Cumberlidge, C. Bergemann, M. Sutherland, Y. Maeno, Cur. Appl. Phys. **8**, 304 (2008). doi:10.1016/j.cap.2007.10.020
111. K. Kitagawa, H. Gotou, Y. Yagi, A. Yamada, T. Matsumoto, Y. Uwatoko, M. Takigawa, J. Phys. Soc. Jpn. **79**, 024001 (2010). doi:10.1143/jpsj.79.024001
112. J. Haase, S.K. Goh, T. Meissner, P.L. Alireza, D. Rybicki, Rev. Sci. Instrum. **80**, 073905 (2009). doi:10.1063/1.3183504
113. T. Meissner, S.K. Goh, J. Haase, B. Meier, D. Rybicki, P.L. Alireza, J. Low Temp. Phys. **159**, 284 (2010). doi:10.1007/s10909-009-0131-5
114. K. Hirayama, T. Yamazaki, H. Fukazawa, Y. Kohori, N. Takeshita, J. Phys. Soc. Jpn. **77**, 075001 (2008). doi:10.1143/jpsj.77.075001

115. C.P. Poole, *Electron spin resonance a comprehensive treatise on experimental techniques* (Dover, NY, 1996)
116. J. Sichelschmidt, V.A. Ivanshin, J. Ferstl, C. Geibel, F. Steglich, Phys. Rev. Lett. **91**, 156401 (2003). doi:10.1103/PhysRevLett.91.156401
117. J. Sichelschmidt, J. Wykhoff, T. Gruner, C. Krellner, C. Klingner, C. Geibel, F. Steglich, H.A. Krug von Nidda, D.V. Zakharov, A. Loidl, I. Fazlizhanov, Phys. Rev. B **81**, 205116 (2010). doi:10.1103/PhysRevB.81.205116
118. H. Ohta, T. Sakurai, S. Okubo, M. Saruhashi, T. Kunimoto, Y. Uwatoko, J. Akimitsu, J. Phys.: Condens. Matter **14**, 10637 (2002). doi:10.1088/0953-89844/44/348
119. T. Sakurai, A. Taketani, T. Tomita, S. Okubo, H. Ohta, Y. Uwatoko, Rev. Sci. Instrum. **78**, 65107 (2007). doi:10.1063/1.2746818
120. T. Sakurai, T. Horie, M. Tomoo, K. Kondo, N. Matsumi, S. Okubo, H. Ohta, Y. Uwatoko, K. Kudo, Y. Koike, H. Tanaka, J. Phys.: Conf. Ser. **215**, 012184 (2010). doi:10.1088/1742-6596/215/1/012184
121. A. Amato, Rev. Mod. Phys. **69**, 1119 (1997). doi:10.1103/RevModPhys.69.1119
122. J.E. Sonier, J.H. Brewer, R.F. Kiefl, Rev. Mod. Phys. **72**, 769 (2000). doi:10.1103/RevModPhys.72.769
123. J.E. Sonier, Rep. Prog. Phys. **70**, 1717 (2007). doi:10.1088/0034-4885/70/11/R01
124. D. Andreica, Magnetic phase diagram in some kondo-lattice compounds: microscopic and macroscopic studies. Phd-thesis, ETH Zürich (2001). doi:10.3929/ethz-a-004171645
125. N. Egetenmeyer, J.L. Gavilano, A. Maisuradze, S. Gerber, D.E. MacLaughlin, G. Seyfarth, D. Andreica, A. Desilets-Benoit, A.D. Bianchi, C. Baines, R. Khasanov, Z. Fisk, M. Kenzelmann, Phys. Rev. Lett. **108**, 177204 (2012). doi:10.1103/PhysRevLett.108.177204
126. S. Klotz, M. Braden, J.M. Besson, Hyperfine Interact. **128**, 245 (2000). doi:10.1023/a:1012691801269
127. D. Bloch, J. Paureau, J. Voiron, G. Parisot, Rev. Sci. Instrum. **47**, 296 (1976). doi:10.1063/1.1134606
128. S.P. Besedin, I.N. Makarenko, S.M. Stishov, V.P. Glazkov, I.N. Goncharenko, V.A. Somenkov, High Press. Res. **14**, 193 (1995). doi:10.1080/08957959508200918
129. S. Klotz, J.M. Besson, G. Hamel, R.J. Nelmes, J.S. Loveday, W.G. Marshall, High Press. Res. **14**, 249 (1996). doi:10.1080/08957959608201409
130. I.N. Goncharenko, High Press. Res. **24**, 193 (2004). doi:10.1080/08957950410001661882
131. C.L. Bull, M. Guthrie, S. Klotz, J. Philippe, T. Strässle, R.J. Nelmes, J.S. Loveday, G. Hamel, High Press. Res. **25**, 229 (2005). doi:10.1080/08957950500452893
132. I.N. Goncharenko, High Press. Res. **27**, 187 (2007). doi:10.1080/08957950601105507
133. J. Paureau, C. Vettier, Rev. Sci. Instrum. **46**, 1484 (1975). doi:10.1063/1.1134083
134. W. Bao, C. Broholm, S.F. Trevino, Rev. Sci. Instrum. **66**, 1260 (1995). doi:10.1063/1.1146019
135. F. Amita, A. Onodera, Rev. Sci. Instrum. **69**, 2738 (1998). doi:10.1063/1.1149008
136. B. Fåk, D.F. McMorrow, P.G. Niklowitz, S. Raymond, E. Ressouche, J. Flouquet, P.C. Canfield, S.L. Budko, Y. Janssen, M.J. Gutmann, J. Phys.: Condens. Matter **17**, 301 (2005). doi:10.1088/0953-89847/2/006
137. W. Wang, D.A. Sokolov, A.D. Huxley, K.V. Kamenev, Rev. Sci. Instrum. **82**, 073903 (2011). doi:10.1063/1.3608112
138. S. Klotz, *Techniques in High Pressure Neutron Scattering* (CRC Press, Boca Raton, 2012)
139. M.M. Abd-Elmeguid, Hyperfine Interact. **113**, 111 (1998). doi:10.1023/A:1012615414512
140. S. Medvedev, T.M. McQueen, I.A. Troyan, T. Palasyuk, M.I. Eremets, R.J. Cava, S. Naghavi, F. Casper, V. Ksenofontov, G. Wortmann, C. Felser, Nature Mater. **8**, 630 (2009). doi:10.1038/nmat2491
141. J.S. Schilling, U.F. Klein, W.B. Holzapfel, Rev. Sci. Instrum. **45**, 1353 (1974). doi:10.1063/1.1686499
142. G.R. Hearne, M.P. Pasternak, R.D. Taylor, Hyperfine Interact. **92**, 1155 (1994). doi:10.1007/bf02065748
143. G.R. Hearne, M.P. Pasternak, R.D. Taylor, Rev. Sci. Instrum. **65**, 3787 (1994). doi:10.1063/1.1144508

144. L. Degiorgi, Rev. Mod. Phys. **71**, 687 (1999). doi:10.1103/RevModPhys.71.687
145. H. Okamura, M. Matsunami, R. Kitamura, S. Ishida, A. Ochiai, T. Nanba, J. Phys.: Conf. Ser. **215**, 012051 (2010). doi:10.1088/1742-6596/215/1/012051
146. L. Degiorgi, New J. Phys. **13**, 023011 (2011). doi:10.1088/1367-2630/13/2/023011
147. A.F. Goncharov, Int. J. Spectr. **2012**, 617528 (2012). doi:10.1155/2012/617528
148. Y. Syuma, M. Keizo, Sci. Technol. Adv. Mater. **10**, 024307 (2009). doi:10.1088/1468-6996/10/2/024307
149. M. Lang, J. Müller, *Organic Superconductors Superconductivity* (Springer, Berlin, 2008), p. 1155. doi:10.1007/978-3-540-73253-2-20
150. G.R. Stewart, Rev. Mod. Phys. **83**, 1589 (2011). doi:10.1103/RevModPhys.83.1589
151. F. Steglich, J. Aarts, C.D. Bredl, W. Lieke, D. Meschede, W. Franz, H. Schäfer, Phys. Rev. Lett. **43**, 1892 (1979). doi:10.1103/PhysRevLett.43.1892
152. B. Bellarbi, D. Jaccard, A. Benoit, J.M. Mignot, H.F. Braun, Phys. Rev. B **30**, 1182 (1984). doi:10.1103/PhysRevB.30.1182
153. F. Thomas, F. Thomasson, C. Ayache, C. Geibel, F. Steglich, Phys. B **303**, 168–188 (1993). doi:10.1016/0921-4526(93)90561-j
154. F. Thomas, C. Ayache, I.A. Fomine, J. Thomasson, C. Geibel, J. Phys.: Condens. Matter **8**, L51 (1996). doi:10.1088/0953-8984/8/4/002
155. H.Q. Yuan, F.M. Grosche, M. Deppe, C. Geibel, G. Sparn, F. Steglich, Science **302**, 2104 (2003). doi:10.1126/science.1091648
156. D. Jaccard, K. Behnia, J. Sierro, Phys. Lett. A **163**, 475 (1992). doi:10.1016/0375-9601(92)90860-o
157. R. Movshovich, T. Graf, D. Mandrus, J.D. Thompson, J.L. Smith, Z. Fisk, Phys. Rev. B **53**, 8241 (1996). doi:10.1103/PhysRevB.53.8241
158. N.D. Mathur, F.M. Grosche, S.R. Julian, I.R. Walker, D.M. Freye, R.K.W. Haselwimmer, G.G. Lonzarich, Nature **394**, 39 (1998). doi:10.1038/27838
159. F.M. Grosche, S.R. Julian, N.D. Mathur, G.G. Lonzarich, Phys. B **50**, 223–224 (1996). doi:10.1016/0921-4526(96)00036-1
160. J.D. Thompson, N. Nicklas, A. Bianchi, R. Movshovich, A. Llobet, W. Bao, A. Malinowski, M.F. Hundley, N.O. Moreno, P.G. Pagliuso, J.L. Sarrao, S. Nakatsuji, Z. Fisk, R. Borth, E. Lengyel, N. Oeschler, G. Sparn, F. Steglich, Phys. B **446**, 329–333 (2003). doi:10.1016/s0921-4526(02)01987-7
161. A. Llobet, J.S. Gardner, E.G. Moshopoulou, J.M. Mignot, M. Nicklas, W. Bao, N.O. Moreno, P.G. Pagliuso, I.N. Goncharenko, J.L. Sarrao, J.D. Thompson, Phys. Rev. B **69**, 24403 (2004). doi:10.1103/PhysRevB.69.024403
162. M. Nicklas, R. Borth, E. Lengyel, P.G. Pagliuso, J.L. Sarrao, V.A. Sidorov, G. Sparn, F. Steglich, J.D. Thompson, J. Phys.: Condens. Matter **13**, L905 (2001). doi:10.1088/0953-89843/4404
163. T. Muramatsu, N. Tateiwa, T.C. Kobayashi, K. Shimizu, K. Amaya, D. Aoki, H. Shishido, Y. Haga, Y. Ōnuki, J. Phys. Soc. Jpn. **70**, 3362 (2001). doi:10.1143/jpsj.70.3362
164. V.A. Sidorov, M. Nicklas, P.G. Pagliuso, J.L. Sarrao, Y. Bang, A.V. Balatsky, J.D. Thompson, Phys. Rev. Lett. **89**, 157004 (2009). doi:10.1103/PhysRevLett.89.157004
165. H. Hegger, H.G. Moshopoulou, M.F. Hundley, J.L. Sarrao, Z. Fisk, J.D. Thompson, Phys. Rev. Lett. **84**, 4986 (2000). doi:10.1103/PhysRevLett.84.4986
166. C. Petrovic, P.G. Pagliuso, M.F. Hundley, R. Movshovich, J.L. Sarrao, J.D. Thompson, Z. Fisk, P. Monthoux, J. Phys.: Condens. Matter **13**, L337 (2001). doi:10.1088/0953-89843703
167. C. Petrovic, R. Movshovich, M. Jaime, P.G. Pagliuso, M.F. Hundley, J.L. Sarrao, J.D. Thompson, Z. Fisk, Europhys. Lett. **53**, 354 (2001). doi:10.1209/epl/i2001-00161-8
168. R. Movshovich, M. Jaime, J.D. Thompson, C. Petrovic, Z. Fisk, P.G. Pagliuso, J.L. Sarrao, Phys. Rev. Lett. **86**, 5152 (2001). doi:10.1103/PhysRevLett.86.5152
169. L.D. Pham, T. Park, S. Maquilon, J.D. Thompson, Z. Fisk, Phys. Rev. Lett. **97**, 056404 (2006). doi:10.1103/PhysRevLett.97.056404

170. M. Nicklas, O. Stockert, P. Tuson, K. Habicht, K. Kiefer, L.D. Pham, J.D. Thompson, Z. Fisk, F. Steglich, Phys. Rev. B **76**, 052401 (2007). doi:10.1103/PhysRevB.76.052401
171. S. Nair, O. Stockert, U. Witte, M. Nicklas, R. Schedler, K. Kiefer, J.D. Thompson, A.D. Bianchi, Z. Fisk, S. Wirth, F. Steglich, Proc. Natl. Acad. Sci. USA 107, 9537 (2010). doi:10.1073/pnas.1004958107
172. M. Nicklas, V.A. Sidorov, H.A. Borges, P.G. Pagliuso, J.L. Sarrao, J.D. Thompson, Phys. Rev. B **70**, 20505 (2004). doi:10.1103/PhysRevB.70.020505
173. T. Muramatsu, T.C. Kobayashi, K. Shimizu, K. Amaya, D. Aoki, Y. Haga, Y. Ōnuki, Phys. C **539**, 388–389 (2003). doi:10.1016/s0921-4534(02)02731-4
174. P.G. Pagliuso, C. Petrovic, R. Movshovich, D. Hall, M.F. Hundley, J.L. Sarrao, J.D. Thompson, K. Fisk, Phys. Rev. B **64**, 100503 (2001). doi:10.1103/PhysRevB.64.100503
175. A. Bianchi, R. Movshovich, C. Capan, P.G. Pagliuso, J.L. Sarrao, Phys. Rev. Lett. **91**, 187004 (2003). doi:10.1103/PhysRevLett.91.187004
176. H.A. Radovan, N.A. Fortune, T.P. Murphy, S.T. Hannahs, E.C. Palm, S.W. Tozer, D. Hall, Nature **425**, 51 (2003). doi:10.1038/nature01842
177. P. Fulde, R.A. Ferrell, Phys. Rev. **135**, A550 (1964). doi:10.1103/PhysRev.135.A550
178. A.I. Larkin, Y.N. Ovchinnikov, Zh Eksp, Teor. Fiz. **47**, 1136 (1964)
179. F. Ronning, C. Capan, E.D. Bauer, J.D. Thompson, J.L. Sarrao, R. Movshovich, Phys. Rev. B **73**, 64519 (2006). doi:10.1103/PhysRevB.73.064519
180. S. Singh, C. Capan, M. Nicklas, M. Rams, A. Gladun, H. Lee, J.F. DiTusa, Z. Fisk, F. Steglich, S. Wirth, Phys. Rev. Lett. **98**, 057001 (2007). doi:10.1103/PhysRevLett.98.057001
181. C.F. Miclea, M. Nicklas, D. Parker, K. Maki, J.L. Sarrao, J.D. Thompson, G. Sparn, F. Steglich, Phys. Rev. Lett. **96**, 117001 (2006). doi:10.1103/PhysRevLett.96.117001
182. M. Nicklas, C.F. Miclea, J.L. Sarrao, J.D. Thompson, G. Sparn, F. Steglich, J. Low Temp. Phys. **146**, 669 (2007). doi:10.1007/s10909-006-9284-7
183. M. Kenzelmann, T. Strässle, C. Niedermayer, M. Sigrist, B. Padmanabhan, M. Zolliker, A.D. Bianchi, R. Movshovich, E.D. Bauer, J.L. Sarrao, J.D. Thompson, Science **321**, 1652 (2008). doi:10.1126/science.1161818